

Facile and fast growth of high mobility nanoribbons of $ZrTe_5$

Jingyue Wang(王璟岳), Jingjing Niu(牛晶晶), Xinqi Li(李新祺), Xiumei Ma(马秀梅), Yuan Yao(姚湲), Xiaosong Wu(吴孝松)

Citation: Chin. Phys. B . 2020, 29(6): 068102 . **doi:** 10.1088/1674-1056/ab889a
Journal homepage: http://cpb.iphy.ac.cn; http://iopscience.iop.org/cpb

What follows is a list of articles you may be interested in

A low-dimensional crystal growth model on an isotropic and quasi-free sustained substrate

Chenxi Lu(卢晨曦), Senjiang Yu(余森江), Lingwei Li(李领伟), Bo Yang(杨波), Xiangming Tao(陶向明), Gaoxiang Ye(叶高翔)

Chin. Phys. B . 2020, 29(3): 038101 . **doi:** 10.1088/1674-1056/ab6968

A numerical study on pattern selection in crystal growth by using anisotropic lattice Boltzmann-phase field method

Zhaodong Zhang(张兆栋), Yuting Cao(曹宇婷), Dongke Sun(孙东科), Hui Xing(邢辉), Jincheng Wang(王锦程), Zhonghua Ni(倪中华)

Chin. Phys. B . 2020, 29(2): 028103 . **doi:** 10.1088/1674-1056/ab6718

Multiple enlarged growth of single crystal diamond by MPCVD with PCD-rimless top surface

Ze-Yang Ren(任泽阳), Jun Liu(刘俊), Kai Su(苏凯), Jin-Feng Zhang(张金凤), Jin-Cheng Zhang(张进成), Sheng-Rui Xu(许晟瑞), Yue Hao(郝跃)

Chin. Phys. B . 2019, 28(12): 128103 . **doi:** 10.1088/1674-1056/ab53cd

Effect of growth temperature of $GaAs_xSb_{1-x}$ metamorphic buffer layer on electron mobility of InAs/AlSb heterostructures grown on Si substrate

Jing Zhang(张静), Hong-Liang Lv(吕红亮), Hai-Qiao Ni(倪海桥), Shi-Zheng Yang(杨施政), Xiao-Ran Cui(崔晓然), Zhi-Chuan Niu(牛智川), Yi-Men Zhang(张义门), Yu-Ming Zhang(张玉明)

Chin. Phys. B . 2019, 28(11): 118102 . **doi:** 10.1088/1674-1056/ab4d49

Thin-film growth behavior of non-planar vanadium oxide phthalocyanine

Tian-Jiao Liu(刘天娇), Hua-Yan Xia(夏华艳), Biao Liu(刘标), Tim S Jones, Mei Fang(方梅), Jun-Liang Yang(阳军亮)

Chin. Phys. B . 2019, 28(8): 088101 . **doi:** 10.1088/1674-1056/28/8/088101

RAPID COMMUNICATION

Facile and fast growth of high mobility nanoribbons of $ZrTe_5$*

Jingyue Wang(王璟岳)[1], Jingjing Niu(牛晶晶)[1], Xinqi Li(李新祺)[1], Xiumei Ma(马秀梅)[1], Yuan Yao(姚湲)[2], and Xiaosong Wu(吴孝松)[1,3,4,†]

[1] *State Key Laboratory for Artificial Microstructure and Mesoscopic Physics, Peking University, Beijing* 100871, *China*
[2] *Institute of Physics, Chinese Academy of Sciences, Beijing* 100190, *China*
[3] *Frontiers Science Center for Nano-optoelectronics and Collaborative Innovation Center of Quantum Matter, Peking University, Beijing* 100871, *China*
[4] *Department of Physics, South University of Science and Technology of China, Shenzhen* 518055, *China*

(Received 9 March 2020; revised manuscript received 2 April 2020; accepted manuscript online 11 April 2020)

Recently, $ZrTe_5$ has received a lot of attention as it exhibits various topological phases, such as weak and strong topological insulators, a Dirac semimetal, a three-dimensional quantum Hall state, and a quantum spin Hall insulator in the monolayer limit. While most of studies have been focused on the three-dimensional bulk material, it is highly desired to obtain nanostructured materials due to their advantages in device applications. We report the synthesis and characterizations of $ZrTe_5$ nanoribbons. Via a silicon-assisted chemical vapor transport method, long nanoribbons with thickness as thin as 20 nm can be grown. The growth rate is over an order of magnitude faster than the previous method for the bulk crystals. Moreover, transport studies show that the nanoribbons are of low unintentional doping and high carrier mobility, over 30000 $cm^2/V{\cdot}s$, which enable reliable determination of the Berry phase of π in the *ac* plane from quantum oscillations. Our method holds great potential in growth of high quality ultra-thin nanostructures of $ZrTe_5$.

Keywords: $ZrTe_5$ nanoribbons, growth, chemical vapor transport, mobility

PACS: 81.10.–h, 73.63.–b, 73.23.–b **DOI:** 10.1088/1674-1056/ab889a

1. Introduction

The discovery of topological insulators (TI) has brought a new insight into the classification of solid state materials and attracted enormous interest in the past few years.[1,2] Soon, the topological concept has been extended to superconductors and metals, i.e., three-dimensional (3D) topological Dirac semimetals and Weyl semimetals.[1–10] Among many topological materials, $ZrTe_5$ is unique in that it exhibits various topological phases, such as weak and strong topological insulators, a Dirac semimetal, a 3D quantum Hall state, and a quantum spin Hall insulator in the monolayer limit.[11–22] These phases sensitively depend on the lattice constants.[23] The change of the band structure with temperature, thickness, and pressure has been experimentally observed.[24–28]

Most of studies on $ZrTe_5$ have been carried out for 3D bulk.[15,16,18,29,30] On the other hand, nanowires/nanoribbons of topological materials can be very useful, as they not only enhance the contribution from the surface states due to a large surface-to-volume ratio, but also give rise to new properties.[31–33] For instance, studies on nanostructured topological insulators have revealed interesting phases and spin related transport.[34–36] The marriage between InSb nanowires and superconductors has given birth to the experimental realization of Majarona zero modes.[37] It is therefore highly desired to develop methods for growth of high quality nanostructured $ZrTe_5$ so that new properties may be further introduced. However, such a study has so far not been reported.

Conventionally, $ZrTe_5$ is synthesized by a chemical vapor transport method. The growth is time-consuming, in the order of weeks, which hinders efforts on improvement of the crystal quality.[15,17,38,39] In this work, we employ a silicon-assisted chemical vapor transport method to grow both $ZrTe_5$ nanoribbons and bulk crystals. The growth time of millimeter size single crystals is reduced to less than 90 min, representing substantial improvement of the growth rate. Quantum transport measurements show that the as-grown nanoribbons are of high mobility and low unintentional doping. Well-resolved quantum oscillations confirm a topological band with a Berry phase π in the *ac* plane. Our method holds great potential in growth of ultra-thin nanostructures and bulk crystals of $ZrTe_5$.

2. Growth method

Growth was carried out in a horizontal three-zone tube furnace. The source materials are zirconium and tellurium elements. Since zirconium powder is difficult to handle as it is easily oxidized and flammable, shots of 0.6 g each on average were used instead. Considering much less surface area of shots than powder, the amount of zirconium was significantly more than the stoichiometric ratio, e.g., 5 g Zr and 0.3 g Te. Iodine of 2 mg/cm^3 was employed as the transport agent. As

*Project supported by the National Key Research and Development Program of China (Grant Nos. 2016YFA0300600, 2016YFA0300802, 2013CB932904, and 2016YFA0202500) and the National Natural Science Foundation of China (Grant Nos. 11574005, 11774009, and 11234001).

†Corresponding author. E-mail: xswu@pku.edu.cn

© 2020 Chinese Physical Society and IOP Publishing Ltd

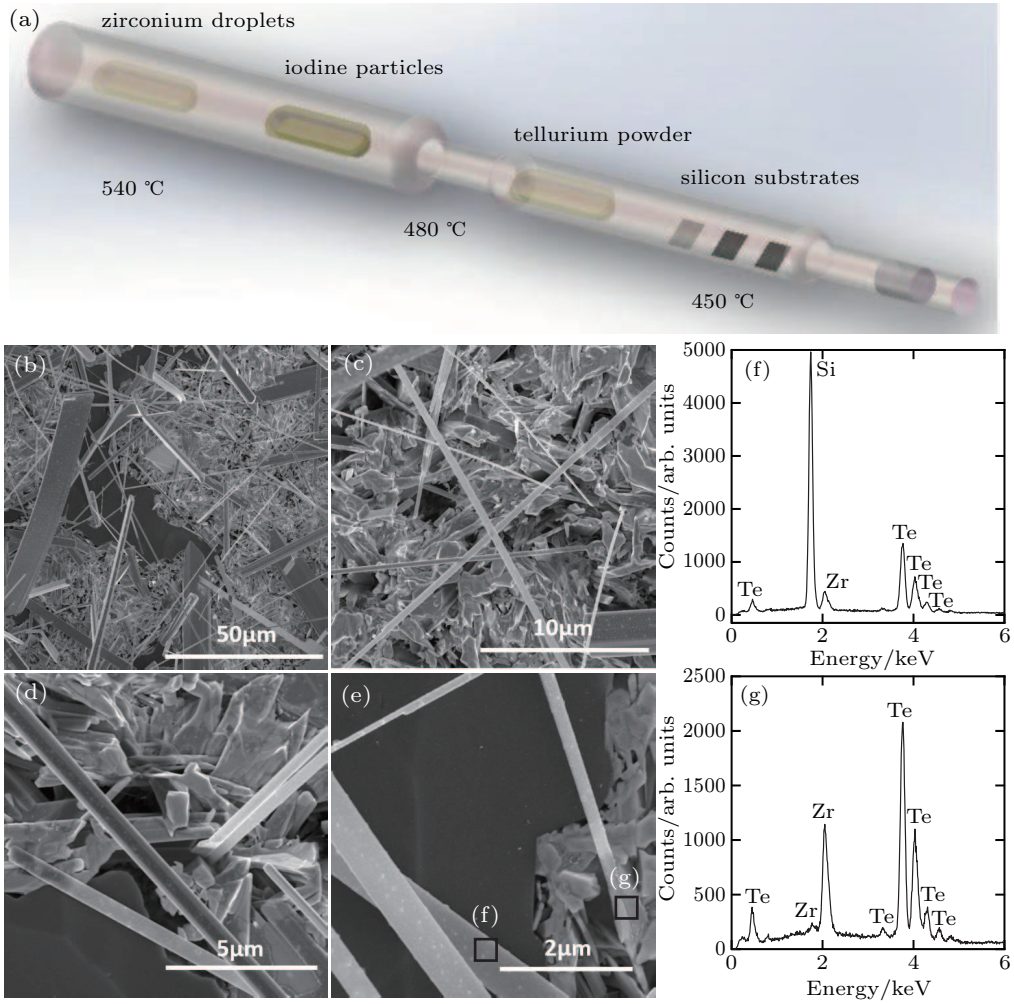


Fig. 1. Growth of $ZrTe_5$ nanostructures. (a) A schematic drawing of the growth setup for the iodine vapor transport method. A two-bulb ampoule is used. Zirconium shots and iodine particles are placed in one bulb, which is held at a higher temperature, 540 ℃. Tellurium powder and silicon substrates are placed in the other bulb, which is held at a lower temperature, 480 ℃ and 450 ℃, respectively. (b)–(e) A series of SEM images of grown nanostructures with increasing magnifications. $ZrTe_5$ nanoribbons are grown on a mattress of $ZrTe_3$ and Te crystals. A recession of the silicon substrate due to iodine etching can be observed in (d) and (e). (f) Energy-dispersive x-ray spectroscopy of nanoribbon, indicating $ZrTe_5$. (g) A spectrum taken at the root of the nanoribbon, indicating $ZrTe_3$. The black squares in (e) mark the spots where the spectra were taken.

illustrated in Fig. 1(a), the source materials, iodine, and several growth substrates were sealed in a quartz ampoule. The size of each silicon substrate is 1 cm×1 cm×0.5 mm. The total length of the ampoule is around 60 cm. The distance between zirconium shots and the nearest substrate is around 50 cm, the distance from tellurium powder to the nearest substrate is around 15 cm. Before sealing, the ampoule was flushed by argon and pumped to 5 Pa before the growth process. The effect of residual gas on the transport of chemical species during reaction is negligible as the partial pressure is orders of magnitude lower than that of iodine (and its gaseous compound) and tellurium. In particular, zirconium shots and iodine particles were placed in one side of the ampoule, while tellurium powder and silicon substrates were placed in the other side. The iodine vapor transport growth of $ZrTe_5$ can be qualitatively described by the following reactions:

$$\mathrm{Zr} + 2\mathrm{I_2} \rightarrow \mathrm{ZrI_4},$$
$$\mathrm{ZrI_4} + 5\mathrm{Te} \rightarrow \mathrm{ZrTe_5} + 2\mathrm{I_2}.$$

Due to the low vapor pressure of Zr, the first reaction was set in the highest temperature zone, so sufficient ZrI_4 could be fed to the second reaction, which was held in the lowest temperature zone. The tellurium powder was placed in the third temperature zone in between the other two zones. The optimal temperatures of the three zones were found to be 540 ℃, 480 ℃, and 450 ℃, respectively. The growth usually took place for 150 min to grow nanostructures (or 90 min for bulk at the coldest part of the quartz ampoule), and then the ampoule was allowed to cool naturally.

3. Results

3.1. Morphology of $ZrTe_5$ nanoribbons

Nanoribbons were found on the silicon substrate and certain segments of the ampoule wall, as shown by the SEM image in Fig. 1. These nanostructures can be very long, e.g., 200 μm. Later we will show via scanning transmission electron microscopy (STEM) and Raman spectroscopy that these

long nanostructures are $ZrTe_5$. A substantial advantage of our method is the fast growth rate. Depending on the growth conditions, such as the ratio and the temperature of the source materials, macroscopic crystals can also been grown in similar growth time on the ampoule wall. The size of the crystals can be as large as 10 mm by 0.2 mm by 0.05 mm, rivalling reported results with several weeks of growth time.[15,38,39] A rough estimation yields a growth rate being at least 40 times faster.

Interestingly, these $ZrTe_5$ nanostructures did not directly grow on the silicon substrate, but on a mattress of materials, as seen in Fig. 1(b). Energy-dispersive x-ray spectroscopy (EDX) measurements show that the mattress mainly consists of Zr and Te with a ratio of $\sim 1:3$, indicating $ZrTe_3$ as seen in Fig. 1(g). Some tellurium crystals were also found. Apparently, $ZrTe_3$ and Te crystals grow first. They may provide a suitable substrate for subsequent growth of $ZrTe_5$. A close look at the edge of the mattress, as shown in Figs. 1(d) and 1(e), reveals recess etching into the silicon substrate. Iodine is known to react with silicon and forms SiI_4, which is in a gaseous phase at our growth temperature. We have found that silicon plays an important role in the reaction. When the silicon substrate was replaced with mica, neither $ZrTe_3$ nor $ZrTe_5$ was formed under the same growth condition. On the other hand, in presence of both silicon and mica substrates, growth could occur on the mica substrate, though much less effectively as shown in Figs. 2(e) and 2(f). How silicon affects the growth processes is not clear currently and deserves further study. In the following, we focus on the quality of the grown nanoribbons.

3.2. High quality of $ZrTe_5$ nanoribbons

EDX was carried out for the nanoribbons, which indicates that they consist of Zr and Te. The atomic ratio is about $1:5$ (within 0.5% error). High-angle annular dark-field (HAADF) images were taken with the aberration corrected transmission electron microscope (JEOL ARM200 F). Figure 2 shows an image of a typical nanoribbon. The most prominent feature is the vertical arrow-like atomic chains. The image matches well with the expected atomic arrangement of the (110) plane of $ZrTe_5$ depicted in the inset of Fig. 2(a), proving that these nanostructures are $ZrTe_5$. The electron diffraction pattern looking down the [110] and [010] directions in Figs. 2(b) and 2(d) also agrees well with $ZrTe_5$. Furthermore, we find that the lattice constants, $a = 0.40$ nm, $b = 1.45$ nm, and $c = 1.34$ nm, are very closed to the expected values for $ZrTe_5$ as well.[12,15,23,24] From these images, it can be seen that the grown samples are of high crystalline quality.

All data show that the nanoribbons are along the a-axis, and the shortest dimension is along the b-axis. This growth mode is in fact expected considering the crystal structure. $ZrTe_5$ is a layered material coupled by Van der Waals interactions, which favors 2D growth in principle. In each layer, there is a strong structural anisotropy, which leads to the dimension along the a-axis being significantly longer than the other dimension (along the c-axis).

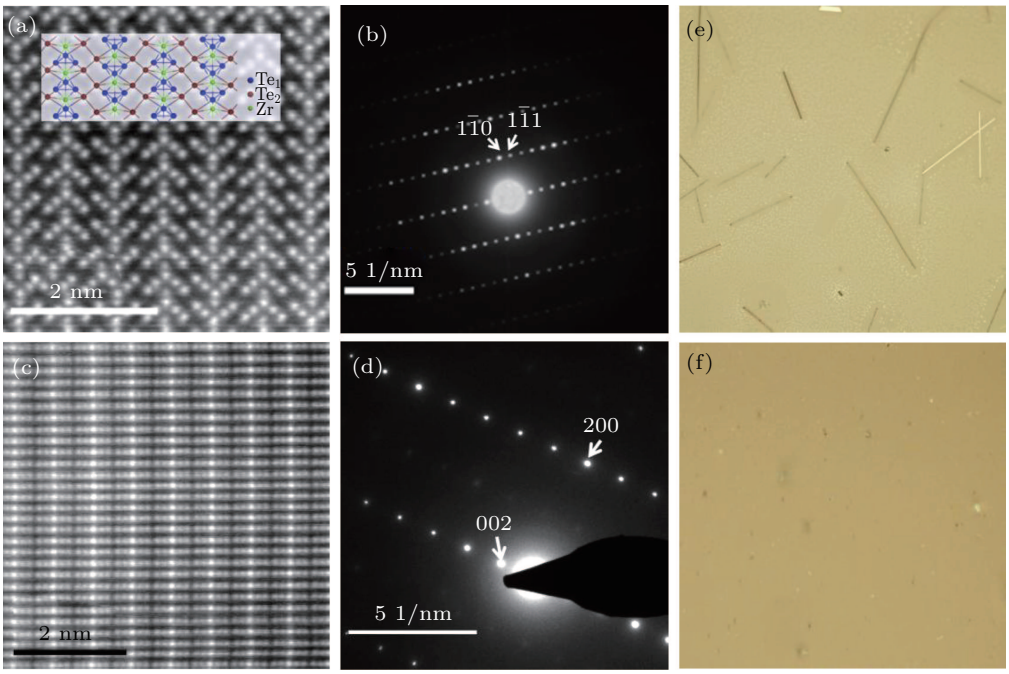


Fig. 2. (a)–(d) Aberration corrected TEM images of $ZrTe_5$ nanoribbon. The nanoribbon is about 50 nm thick. (a) HAADF image. Inset, atomic structure model of $ZrTe_5$ in the (110) plane. (c) HAADF image in the (010) plane. (b), (d) Electron diffraction pattern along the [110] and [010] directions. (e) Optical micrograph of a mica substrate after growth in presence of a silicon substrate. $ZrTe_5$ ribbons can be found. (f) Optical micrograph of a mica substrate after growth without a silicon substrate. No $ZrTe_5$ can be found.

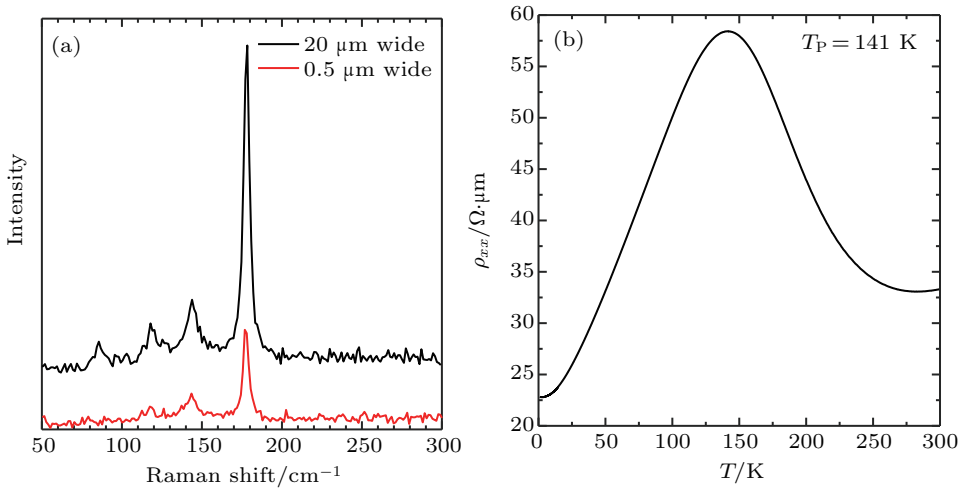


Fig. 3. (a) Raman spectra of $ZrTe_5$ nanoribbons. Four peaks at 115 cm^{-1}, 119 cm^{-1}, 145 cm^{-1}, and 179 cm^{-1} are well resolved in the 20 μm wide ribbon, while the signal is weaker in the 0.5 μm wide ribbon. (b) Temperature dependence of resistivity for a 10 μm×400 nm×90 nm $ZrTe_5$ nanoribbon. A broad maximum appears at $T_P = 141$ K.

Raman spectroscopic measurements were performed. The Raman spectra for narrow and wide nanoribbons are similar, except that the narrow ones have a weaker signal due to a smaller volume to interact with light. Four characteristic peaks, centered at 115 cm^{-1}, 119 cm^{-1}, 145 cm^{-1}, and 179 cm^{-1}, can be readily identified as the vibration modes of Te atoms.[40] The peak positions agree with those of the bulk as shown in Fig. 3(a).

3.3. Transport measurements

The temperature dependence of resistivity of the nanoribbons, shown in Fig. 3(b), exhibits a maximum at 141 K. Such a nonmonotonic behavior is characteristic for $ZrTe_5$.[29,41–44] It origins from a temperature-induced Lifshitz transition.[27] The temperature of the resistivity maximum indicates a boundary between a strong topological insulator and a weak one.[45]

The quality of the nanoribbon is manifested in electrical transport. We have carried out magnetoresistance (MR) measurements under magnetic fields in different directions, as depicted in Fig. 4. The current is always along the nanoribbon, the a-axis. When the field is perpendicular to the current, MR is significant, while it is very small when the field is parallel to the current. In all three field directions, MR displays marked oscillations, the so-called Shubnikov–de Haas oscillations (SdHOs). Surprisingly, SdHOs start to appear in a field $B_{\min}$ as low as 0.34 T as shown in Fig. 4(e), which suggests a high electrical mobility.[46] Due to difficulties in measuring the Hall of a nanoribbon, we estimate the mobility by the following method. Note that SdHOs stem from formation of Landau levels, which requires a condition of $\omega_c\tau > 1$. Here ω_c is the cyclotron frequency, and τ is the mean free time. It is easy to show that the condition is equivalent to $\omega_c\tau = \mu B > 1$, where μ is the mobility. Plugging $B_{\min} = 0.34$ T, we have $\mu > 3\times10^4$ cm$^2\cdot$V$^{-1}\cdot$s^{-1}. The high mobility is beneficial in studying the transport properties of this topological material. Therefore, our work provides a promising growth method for high mobility nanostructured $ZrTe_5$.

In Fig. 4(c), it can be seen that the quantum limit is reached at a relatively small field, 5.5 T, indicating a low carrier density. The low doping level also suggests high quality of the sample, corroborating with other measurements. After subtracting a smooth background, the oscillations are clearly resolved, as shown in Figs. 4(f)–4(h). By picking the field positions of the maxima and minima of the oscillations and plotting the inverse position against the Landau level index n, we obtain the Landau plot, shown in Fig. 5(c). Here, the maxima are assigned integer indices, while the minima are assigned half integer indices. Under this convention, an intercept of $\gamma_b \approx 0.143$ on the y-axis is estimated from a linear fit when $\boldsymbol{B} \parallel b$. The intercept of the Landau plot has been widely used to determine the non-trivial Berry phase of π for topological systems.[47] For a 2D Dirac system, like graphene, $\gamma = 0$, while for 3D materials with a topological nontrivial band, the intercept is expected to be $\pm1/8$.[12,16,30,47] Meanwhile, the intercepts of the Landau plots in $\boldsymbol{B} \parallel a$ and $\boldsymbol{B} \parallel c$ are $\gamma_a \approx 0.679$ and $\gamma_c \approx 0.603$, respectively, which are consistent with other reports.[22,30,48] The difference in the intercept for different field directions is caused by the spin zero effect.[48] Therefore, our data are in excellent agreement with a topological nontrivial system, confirming previous studies.[9,10,48,49]

The slope of the linear dependence gives the oscillation frequency B_f. For the three magnetic field orientations, $B_f = 30.33$ T, 5.14 T, and 25.67 T, respectively. According to the Lifshitz–Onsager relation, $B_f = \hbar S_e/2\pi e$, where $\hbar$ and e are the reduced Plank constant and the elementary charge, respectively, and S_e is the extremal cross-sectional area of the Fermi surface in a plane normal to the magnetic field. Adopting an ellipsoidal Fermi surface, as suggested in earlier studies,[11,50,51] the Fermi wave vectors along the three principle axes can be estimated as $k_a = 0.115$ nm^{-1}, $k_b = 0.68$ nm^{-1},

and $k_c = 0.135\ \text{nm}^{-1}$. Furthermore, the damping of the oscillation amplitude A with temperature can provide an estimation of the band velocity v_0 of the massless Dirac fermion in the system, based on the Lifshitz–Kosevich relation

$$\frac{A(T)}{A(0)} = \frac{\lambda}{\sinh\lambda}, \quad \lambda = \frac{2\pi^2 k_B T k_F}{e v_0 B}, \tag{1}$$

where k_B is the Boltzmann constant. In Fig. 5(a). $A(T)/A(0)$ for $\boldsymbol{B} \parallel b$ is plotted against temperature for several Landau levels, $n = 1$, 2, and 3. By fitting the plots to Eq. (1), we obtain the velocities along the three directions, $v_0^a \approx 5.15 \times 10^5\ \text{m}\cdot\text{s}^{-1}$, $v_0^b \approx 0.85 \times 10^5\ \text{m}\cdot\text{s}^{-1}$, $v_0^c \approx 4.47 \times 10^5\ \text{m}\cdot\text{s}^{-1}$, in agreement with the values reported by others.[16,22,51] Next by using an energy dispersion for a massive Dirac Fermion $E_F = \sqrt{M^2 + (\hbar v_F k_F)^2}$, where M is the mass induced by the gap, we obtain the Fermi level $E_F = 38.3$ meV. The relatively low Fermi level also indicates that our sample displays a low doping level.

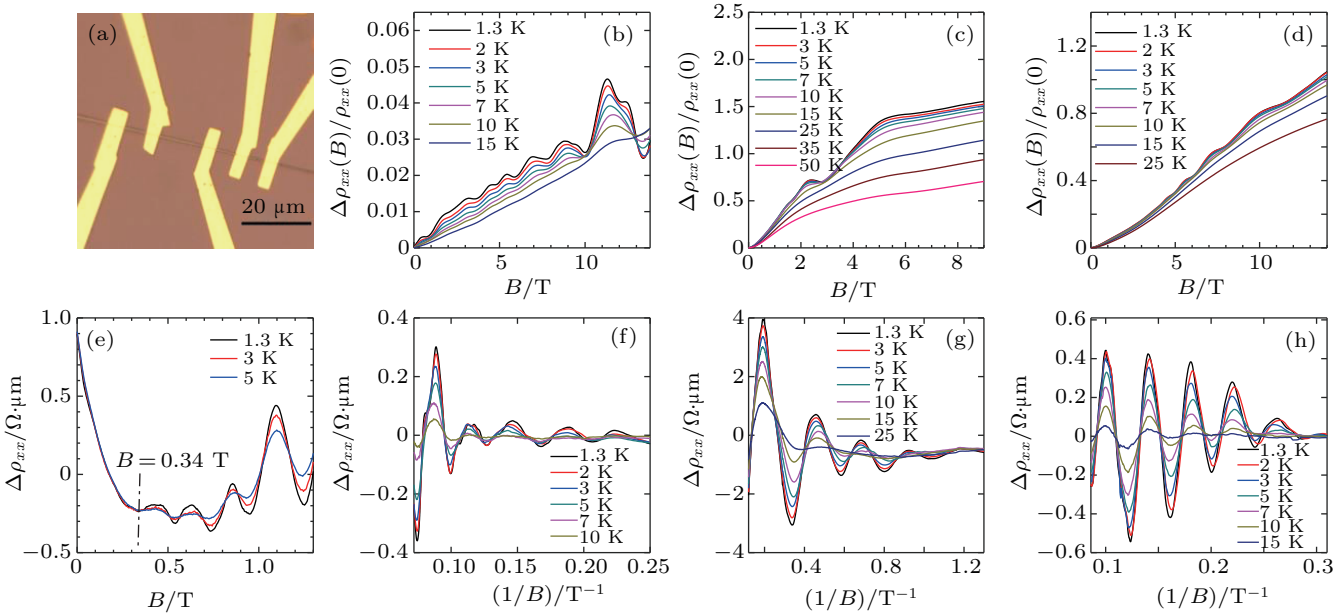


Fig. 4. (a) Optical micrograph of a typical four-point measurement device of a $ZrTe_5$ nanoribbon. Magnetoresistance for a $ZrTe_5$ nanoribbon when (b) $\boldsymbol{B} \parallel a$, (c) $\boldsymbol{B} \parallel b$, (d) $\boldsymbol{B} \parallel c$. (e) Shubnikov–de Haas oscillations appear at low field when $\boldsymbol{B} \parallel b$. (f)–(h) Shubnikov–de Haas oscillations with a smooth background subtracted for fields along the a-, b-, and c-axis.

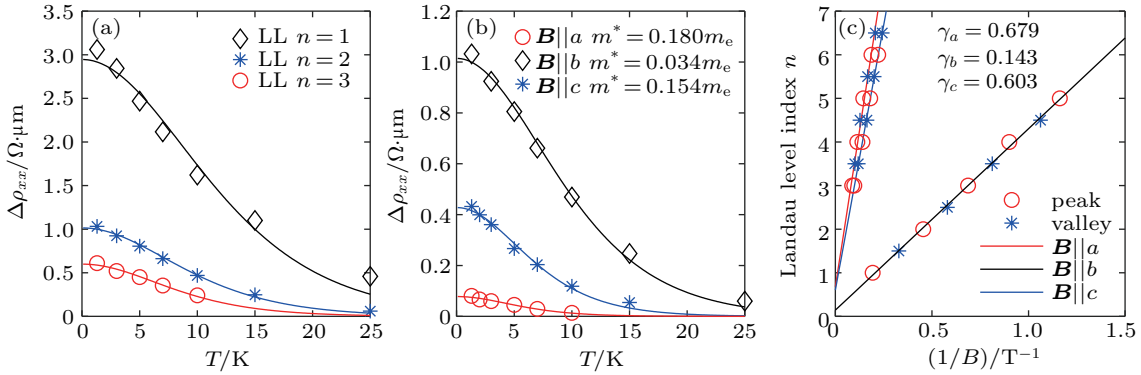


Fig. 5. Analysis of SdH oscillations. (a) Temperature dependence of the oscillation amplitudes. Symbols are experimental data, while lines are best fits to Eq. (1). Black, blue, and red are for Landau levels $n = 1$, $n = 2$, and $n = 3$, respectively. (b) Temperature dependence of the SdH oscillation amplitude for fields along three axes. Open circle, $\boldsymbol{B} \parallel a$; open diamond, $\boldsymbol{B} \parallel b$; asterisk, $\boldsymbol{B} \parallel c$. Solid lines are fits to Eq. (1), from which the cyclotron masses are estimated as $m_a = 0.180m_e$, $m_b = 0.034m_e$, and $m_c = 0.154m_e$. (c) Landau plot of the oscillations. The solid lines are linear fits.

4. Conclusions

We report growth of $ZrTe_5$ nanoribbons by a silicon-assisted chemical vapor transport technique. Compared with the previous growth method for bulk crystals, our technique has the advantage of a fast growth rate. The grown nanoribbons are of high crystalline quality and display low unintentional doping and high mobility, suitable for study of topological properties near the charge neutrality point and beyond the quantum limit. Quantum transport experiments indicate that the $ZrTe_5$ nanoribbon is a topological semimetal with a nontrivial Berry phase π in the ac plane. Our work is the first experiment on growth of $ZrTe_5$ nanostructures and provides a good starting point for studies of nanostructured $ZrTe_5$.

References

[1] Hasan M Z and Kane C L 2010 *Rev. Mod. Phys.* **82** 3045
[2] Qi X L and Zhang S C 2011 *Rev. Mod. Phys.* **83** 1057
[3] Kitaev A 2009 *AIP Conf. Proc.* **1134** 22
[4] Roy R 2008 arXiv:0803.2868 [cond-mat.mes-hall]
[5] Schnyder A P, Ryu S, Furusaki A and Ludwig A W W 2008 *Phys. Rev. B* **78** 195125
[6] Qi X L, Hughes T L, Raghu S and Zhang S C 2009 *Phys. Rev. Lett.* **102** 187001
[7] Wan X, Turner A M, Vishwanath A and Savrasov S Y 2011 *Phys. Rev. B* **83** 205101
[8] Burkov A A and Balents L 2011 *Phys. Rev. Lett.* **107** 127205
[9] Song H D, Sheng D, Wang A Q, Li J G, Yu D P and Liao Z M 2017 *Chin. Phys. B* **26** 037301
[10] Wang H and Wang J 2018 *Chin. Phys. B* **27** 107402
[11] Zheng G, Lu J, Zhu X, Ning W, Han Y, Zhang H, Zhang J, Xi C, Yang J, Du H, Yang K, Zhang Y and Tian M 2016 *Phys. Rev. B* **93** 115414
[12] Yu W, Jiang Y, Yang J, Dun Z L, Zhou H D, Jiang Z, Lu P and Pan W 2016 *Sci. Rep.* **6** 35357
[13] Zhou Y, Wu J, Ning W, Li N, Du Y, Chen X, Zhang R, Chi Z, Wang X, Zhu X, Lu P, Ji C, Wan X, Yang Z, Sun J, Yang W, Tian M, Zhang Y and Mao H 2016 *Proc. Natl. Acad. Sci. USA* **113** 2904
[14] Chen R Y, Zhang S J, Schneeloch J A, Zhang C, Li Q, Gu G D and Wang N L 2015 *Phys. Rev. B* **92** 075107
[15] Li Q, Kharzeev D E, Zhang C, Huang Y, Pletikosic I, Fedorov A V, Zhong R D, Schneeloch J A, Gu G D and Valla T 2016 *Nat. Phys.* **12** 550
[16] Yuan X, Zhang C, Liu Y, Narayan A, Song C, Shen S, Sui X, Xu J, Yu H, An Z, Zhao J, Sanvito S, Yan H and Xiu F 2016 *NPG Asia Mater* **8** e325
[17] Wu R, Ma J Z, Nie S M, Zhao L X, Huang X, Yin J X, Fu B B, Richard P, Chen G F, Fang Z, Dai X, Weng H M, Qian T, Ding H and Pan S H 2016 *Phys. Rev. X* **6** 021017
[18] Pariari A and Mandal P 2017 *Sci. Rep.* **7** 40327
[19] Chen R Y, Chen Z G, Song X Y, Schneeloch J A, Gu G D, Wang F and Wang N L 2015 *Phys. Rev. Lett.* **115** 176404
[20] Manzoni G, Gragnaniello L, Autès G, Kuhn T, Sterzi A, Cilento F, Zacchigna M, Enenkel V, Vobornik I, Barba L, Bisti F, Bugnon Ph, Magrez A, Strocov V N, Berger H, Yazyev O V, Fonin M, Parmigiani F and Crepaldi A 2016 *Phys. Rev. Lett.* **117** 237601
[21] Li X B, Huang W K, Lv Y Y, Zhang K W, Yang C L, Zhang B B, Chen Y B, Yao S H, Zhou J, Lu M H, Sheng L, Li S C, Jia J F, Xue Q K, Chen Y F and Xing D Y 2016 *Phys. Rev. Lett.* **116** 176803
[22] Tang F, Ren Y, Wang P, Zhong R, Schneeloch J, Yang S A, Yang K, Lee P A, Gu G, Qiao Z and Zhang L 2019 *Nature* **569** 537
[23] Weng H, Dai X and Fang Z 2014 *Phys. Rev. X* **4** 011002
[24] Niu J, Wang J, He Z, Zhang C, Li X, Cai T, Ma X, Jia S, Yu D and Wu X 2017 *Phys. Rev. B* **95** 035420
[25] Lu J, Zheng G, Zhu X, Ning W, Zhang H, Yang J, Du H, Yang K, Lu H, Zhang Y and Tian M 2017 *Phys. Rev. B* **95** 125135
[26] Zhang J L, Guo C Y, Zhu X D, Ma L, Zheng G L, Wang Y Q, Pi L, Chen Y, Yuan H Q and Tian M L 2017 *Phys. Rev. Lett.* **118** 206601
[27] Zhang Y, Wang C, Yu L, Liu G, Liang A, Huang J, Nie S, Sun X, Zhang Y, Shen B, Liu J, Weng H, Zhao L, Chen G, Jia X, Hu C, Ding Y, Zhao W, Gao Q, Li C, He S, Zhao L, Zhang F, Zhang S, Yang F, Wang Z, Peng Q, Dai X, Fang Z, Xu Z, Chen C and Zhou X J 2017 *Nat. Commun.* **8** 15512
[28] Tang F, Wang P, Wang P, Gan Y, Wang L, Zhang W and Zhang L 2018 *Chin. Phys. B* **27** 087307
[29] Chi H, Zhang C, Gu G, Kharzeev D E, Dai X and Li Q 2017 *New J. Phys.* **19** 015005
[30] Liu Y, Yuan X, Zhang C, Jin Z, Narayan A, Luo C, Chen Z, Yang L, Zou J, Wu X, Sanvito S, Xia Z, Li L, Wang Z and Xiu F 2016 *Nat. Commun.* **7** 12516
[31] Imura K I, Okamoto M, Yoshimura Y, Takane Y and Ohtsuki T 2012 *Phys. Rev. B* **86** 245436
[32] Qian X, Liu J, Fu L and Li J 2014 *Science* **346** 1344
[33] Zhou J J, Feng W, Liu C C, Guan S and Yao Y 2014 *Nano Lett.* **14** 4767
[34] Zhang Y and Vishwanath A 2010 *Phys. Rev. Lett.* **105** 206601
[35] Peng H L, Lai K J, Kong D S, Meister S, Chen Y L, Qi X L, Zhang S C, Shen Z X and Cui Y 2010 *Nat. Mater.* **9** 225
[36] Hong S S, Zhang Y, Cha J J, Qi X L and Cui Y 2014 *Nano Lett.* **14** 2815
[37] Mourik V, Zuo K, Frolov S M, Plissard S R, Bakkers E P A M and Kouwenhoven L P 2012 *Science* **336** 1003
[38] Sodeck H, Mikler H and Komarek K 1979 *Monatshefte For Chem. Chem. Mon.* **110** 1
[39] Levy F and Berger H 1983 *J. Cryst. Growth* **61** 61
[40] Taguchi I, Grisel A and Levy F 1983 *Solid State Commun.* **46** 299
[41] Okada S, Sambongi T, Ido M, Tazuke Y, Aoki R and Fujita O 1982 *J. Phys. Soc. Jpn.* **51** 460
[42] DiSalvo F J, Fleming R M and Waszczak J 1981 *Phys. Rev. B* **24** 2935
[43] Tritt T M, Lowhorn N D, Littleton R T, Pope A, Feger C R and Kolis J W 1999 *Phys. Rev. B* **60** 7816
[44] Manzoni G, Sterzi A, Crepaldi A, Diego M, Cilento F, Zacchigna M, Bugnon P, Berger H, Magrez A, Grioni M and Parmigiani F 2015 *Phys. Rev. Lett.* **115** 207402
[45] Xu B, Zhao L X, Marsik P, Sheveleva E, Lyzwa F, Dai Y M, Chen G F, Qiu X G and Bernhard C 2018 *Phys. Rev. Lett.* **121** 187401
[46] Wu M, Zhang H, Zhu X, Lu J, Zheng G, Gao W, Han Y, Zhou J, Ning W and Tian M 2019 *Chin. Phys. Lett.* **36** 067201
[47] Murakawa H, Bahramy M S, Tokunaga M, Kohama Y, Bell C, Kaneko Y, Nagaosa N, Hwang H Y and Tokura Y 2013 *Science* **342** 1490
[48] Wang J Y, Niu J J, Yan B M, Li X Q, Bi R, Yao Y, Yu D P and Wu X S 2018 *Proc. Natl. Acad. Sci. USA* **115** 9145
[49] Chen Z G, Chen R Y, Zhong R D, Schneeloch J, Zhang C, Huang Y, Qu F, Yu R, Li Q, Gu G D and Wang N L 2017 *Proc. Natl. Acad. Sci. USA* **114** 816
[50] Kamm G N, Gillespie D J, Ehrlich A C, Wieting T J and Levy F 1985 *Phys. Rev. B* **31** 7617
[51] Zheng G, Zhu X, Lu J, Ning W, Zhang H, Gao W, Han Y, Yang J, Du H, Yang K, Zhang Y and Tian M 2017 *Phys. Rev. B* **96** 121401